PCCP

Accepted Manuscript

ROYAL SOCIETY OF CHEMISTRY

www.rsc.org/pccp

Composition dependent intrinsic defect structures in $SrTiO_3$

Bin Liu [a, *], Valentino R. Cooper [a], Haixuan Xu [b], Haiyan Xiao [b], Yanwen Zhang [a, b], and William J. Weber [b, a, *]

[a]Materials Science and Technology Division, Oak Ridge National Laboratory, Oak Ridge, Tennessee 37831, USA

[b]Department of Materials Science and Engineering, University of Tennessee, Knoxville, Tennessee 37996, USA

*Corresponding authors: Bin Liu, Email: liub2@ornl.gov; William J. Weber, Email: wjweber@utk.edu

Abstract

Intrinsic point defect complexes in $SrTiO_3$ under different chemical conditions are studied using density functional theory. The Schottky defect complex consisting of nominally charged Sr, Ti and O vacancies is predicted to be the most stable defect structure in stoichiometric $SrTiO_3$, with a relatively low formation energy of 1.64 eV/defect. In addition, the mechanisms of defect complex formation in nonstoichiometric $SrTiO_3$ are investigated. Excess SrO leads to the formation of the oxygen vacancies and a strontium-titanium antisite defect, while a strontium vacancy together with an oxygen vacancy and the titanium-strontium antisite defect are produced in an excess TiO_2 environment. Since point defects, such as oxygen vacancies and cation antisite defects, are intimately related to the functionality of $SrTiO_3$, these results provide guidelines for controlling the formation of intrinsic point defects and optimizing the functionality of $SrTiO_3$ by controlling nonstoichiometric chemical compositions of SrO and TiO_2 in experiments.

1 Introduction

Ceramics with the perovskite-type structure (general formula ABO_3) consist of a network of corner-sharing BO_6 octahedra enclosing large cavities, which form higher-coordination sites for the *A*-cations in a roughly cubic array. This structure can accommodate a wide variety of chemical compositions and atomic defects, which have been identified as the origin of the rich variety of phenomena observed in perovskite oxides. As a prototypical perovskite, strontium titanate ($SrTiO_3$) is an ideal model system, due to both its simple cubic symmetry and its wide applications, such as insulating layers in dynamic random-access memories, [1] ferroelectric thin-film structures, [2] high-T_c superconductor substrates, [3] gate oxides [4] and for the immobilization of nuclear waste [5].

In many cases, intrinsic defects can have a significant effect on the properties of $SrTiO_3$. For instance, isolated oxygen vacancies (V_O) and clusters in $SrTiO_3$ are thought to play an important role in the blue and green light emission [6-7] and high *n*-type conductivity [8-9]. In addition, titanium-strontium antisite defects (Ti_{Sr}) have been suggested to be a possible reason for the ferroelectricity and blue light emission observed in $SrTiO_3$ [10]. During crystal growth or film deposition processes, intrinsic defects can be controlled by varying Sr/Ti ratios; inducing substantial differences in properties [11]. For instance, in Nb-doped $SrTiO_3$, with very modest modifications in the Sr/Ti ratio, the conductivity can be tuned by several orders of magnitude, producing either a dark or light colored insulator [11]. Furthermore, through a combination of transmission electron microscopy and first principles calculations, the effect of intrinsic point defects on the grain boundary of $SrTiO_3$ has also been elucidated [12-15]. Here, grain boundaries have been found to be intrinsically nonstoichiometric [13-14]. Such nonstoichiometry is dominated

by various types of point defects at different grain boundaries. These defects play a key role in the stability of grain boundaries; leading to structural distortions and significant changes in material properties [13-15].

The stability of various types of point defects is a focus of the theoretical studies. Theoretical investigations using empirical interatomic potentials have evaluated the energetics of intrinsic point defects in undoped and doped $SrTiO_3$ [16-17]. These studies predicted that the Schottky defect complex, $V_{Sr}^{2-} + V_{Ti}^{4-} + 3V_O^{2+}$, has a much smaller formation energy than Sr, Ti and O Frenkel defect complexes. For dopants, it has been shown that all mono- and divalent cations prefer to substitute at strontium sites, but the substitution sites for trivalent and tetravalent cations are more complex [16]. On the other hand, theoretical investigations of $SrTiO_3$ using first principles calculations have also been performed, but to our knowledge these studies have focused primarily on isolated point defects. Tanaka *et al* studied the energetics of Sr (V_{Sr}), Ti (V_{Ti}) and O (V_O) vacancies, and they found that the relative stability of the defect species is dependent upon the atomic chemical potential. [18] Choi *et al* investigated the energetics of the Ti_{Sr} cation antisite defect and predicted that the Ti_{Sr} antisite defect could be the dominant defect in Ti-rich $SrTiO_3$ as well as V_O [10].

While a great number of experimental and theoretical investigations have been performed, the types and concentrations of possible defect complexes in stoichiometric and nonstoichiometric $SrTiO_3$ remain unverified. In this study, we aim to provide: (1) fundamental and comprehensive insight into the energetics and stability of charged point defect complexes in $SrTiO_3$; and (2) guidelines for the experimental fabrication and optimization of the properties of $SrTiO_3$ through the control of point defect types. This paper is structured as follows: first, we

calculate the energetics of isolated defects in different charged-states, in which the chemical potential environments resulting from $SrTiO_3$ stability limits are considered. Subsequently, the types and concentrations of predominant defect complexes under stoichiometric and nonstoichiometric $SrTiO_3$ are quantitatively analyzed. We predict that the Schottky defect complex consisting of nominally charged Sr, Ti and O vacancies is the most stable defect structure. Furthermore, we predict that specific defect complexes can be obtained by controlling the relative chemical compositions of SrO and TiO_2 during the experimental growth process.

2 Computational details

2.1 DFT calculation details

The VASP (Vienna Ab-Initio Simulation Package) code using the projector augmented wave method is used in the present density functional theory (DFT) calculations [19]. The generalized gradient approximation (GGA) with the exchange correlation potential of Perdew-Burke-Ernzerhof (PBE) is selected [20]. To correct for the on-site Coulomb interaction of the 3*d* orbitals, the rotationally invariant +*U* method [21] is applied with U = 5.0 eV and J = 0.64 eV [7, 22]. All computations are based on a 3 × 3 × 3 supercell consisting of 135 atoms with a 2 × 2 × 2 k-point grid[23] and a cutoff energy of 400 eV for the plane wave basis set. The crystal structures were relaxed until the forces on individual atoms were smaller than 5×10^{-3} eV/Å. Spin polarization was taken into account in all calculations. The calculated lattice constant for bulk $SrTiO_3$ was determined to be 3.93 Å, in typical DFT agreement with the experimental value of a_0 = 3.89 Å [24].

2.2 Point defect formation energy

The defect formation energies, E_f, are evaluated as:

$$E_f = E_d - E_p + \sum n_i \mu_i + q(\Delta E_F + E_{VBM}) \quad (1)$$

where E_d and E_p are the total energies of the defective and defect free supercells, respectively, q is the charge state of the defect, n_i is the number of atoms being removed or added, and μ_i is the corresponding chemical potential. E_{VBM} and ΔE_F are the energy levels corresponding to the valance band maximum (VBM) and the Fermi energy measured from the VBM, respectively. The Fermi energy, ΔE_F, changes its position within the band gap, E_g, which is represented by the energy difference between valance band maximum and the conduction-band minimum (CBM) as $E_g = E_p(-1) + E_p(+1) - 2E_p(0)$, where -1, +1 and 0 are the charge states. The calculated E_g=2.68 eV is smaller than the experimental value of 3.25 eV [25], but is typical of DFT calculations. In our calculations, however, this difference (ΔE_g = 0.57 eV) can considerably affect the computed point defect formation energies [10, 26]. Previous studies have shown that the error in defect formation energies due to the underestimated DFT band gap can be corrected by adding a constant energy shift (in this case 0.57 eV) to the conduction states in order to match the experimental gap [10, 26]. For an isolated defect, it can be assumed that the energy levels of the acceptor-like and the deep donor-like defects follow the VBM and are thus unchanged. On the other hand, shallow donor-like defect levels follow the CBM and are thus shifted upward by the same amount as the band gap [10, 26]. Defect formation energies are corrected accordingly, i.e., no correction is added to the formation energies of the oxygen interstitials, but $m\Delta E_g$ (m is the number of electrons occupying the defect states) is added to the formation energies of the oxygen vacancies [10, 26]. Here, whether a donor level is deep or shallow is determined by checking the one electron energy level in the band gap of the corresponding defect [10].

The thermodynamic transition level of a defect between charge states q and q', $\varepsilon(q/q')$, corresponds to the Fermi energy at which the formation energies for charge states q and q' are

equal. When measured from the VBM, the thermodynamic transition level is given as:

$$\varepsilon(q/q') = \frac{E^{q}_{f,VBM} - E^{q'}_{f,VBM}}{q' - q} \quad (2)$$

where $E^{q}_{f,VBM}$ denotes the defect formation energy for charge state q when the Fermi energy is located at the VBM. The position of the thermodynamic transition level given in equation (2) is the ionization energy of a defect, i.e., the acceptor or donor energy [27].

2.3 Formalism for chemical potential in ternary oxides

As shown in Eq. (1), the formation energy of a defect depends on the chemical potential of the ions added or removed from the perfect crystal to form the defect. A thermodynamically consistent process for determining the experimentally relevant range of chemical potentials is outlined below. This approach was originally developed in the context of binary oxides [28-29] and then extended to ternary oxides, such as Y_2SiO_5 [30-31], $LiNbO_3$ [32] and $Y_3Al_5O_{12}$ [33].

The total energy of a stoichiometric unit of $SrTiO_3$ can be expressed as:

$$\mu_{Sr} + \mu_{Ti} + 3\mu_{O} = \mu_{SrTiO_3} \quad (3)$$

The stability of the system against decomposition into its constituent elements places upper limits on the chemical potential of each element in $SrTiO_3$. The reference substances are pure solids of Sr and Ti, as well as molecular oxygen (O_2). Therefore, additional restrictions are set by:

$$\mu_{Sr} \le \mu^{bulk}_{Sr} \quad (4\text{-}1)$$

$$\mu_{Ti} \le \mu^{bulk}_{Ti} \quad (4\text{-}2)$$

$$\mu_{O} \le \mu^{O_2}_{O} \quad (4\text{-}3)$$

Since neither SrO nor TiO_2 precipitates from bulk $SrTiO_3$, the following restrictions are also included:

$$\mu_{Sr} + \mu_O \leq \mu_{SrO} \quad (5\text{-}1)$$

$$\mu_{Ti} + 2\mu_O \leq \mu_{TiO_2} \quad (5\text{-}2)$$

The above set of equations defines the range of chemical potentials consistent with the stability of $SrTiO_3$ against decomposition into binary oxides or into its elemental components. Given the boundary for the chemical potential of each element, a valid range for the formation energies of the point defects can be examined.

3 Results and discussion

An initial step in studying the energetics of defects is to determine the preferred position of an isolated point defect. As a consequence of the $SrTiO_3$ $Pm\bar{3}m$ symmetry, the structures of atomic vacancies (V_O, V_{Sr} and V_{Ti}) and cation antisite defects (Sr_{Ti} and Ti_{Sr}) are straightforward since there is only one crystallographically inequivalent site for each atom. In contrast, the structures of the interstitial configurations (O_i, Sr_i and Ti_i; here, subscript i means interstitial) are more complex. Our recent *ab initio* molecular dynamic simulation [34] showed that oxygen favors a split-interstitial configuration along the <100> direction (Fig. 1a), with two atoms sharing a single lattice site. Similarly, Sr forms a split-interstitial but along the <111> direction (Fig. 1b). The titanium interstitial (Fig. 1c), however, occupies a bridge site between two Sr atoms along a channel and in-plane with four nearest neighboring Ti and/or O atoms. In the present study, these configurations for O_i, Sr_i and Ti_i are, therefore, investigated.

After comprehensively considering the abovementioned chemical potential restrictions, a well-defined ternary phase diagram of $SrTiO_3$ is determined and shown in Fig.2. This figure depicts a narrow region of stability for $SrTiO_3$, defined by the quadrangle ABCD and restricted

by the Ti, O_2, SrO and TiO_2 precipitation lines. The corner points, A, B, C and D, correspond to Ti- & TiO_2-rich, O- & TiO_2-rich, O- & SrO-rich and Ti- & SrO-rich precipitate phase boundaries, respectively. The values of the chemical potentials for Sr, Ti and O at the corner points are given in Table I.

3.1 Formation energies of isolated point defects

The formation energies of all isolated point defect types with different charge states in $SrTiO_3$ are calculated using Eq. (1). Since the defect formation energies depend on the electron Fermi energy, the influence of the Fermi energy on the stability of each individual defect is considered. The reference zero for the Fermi energy is assigned to be the VBM. For any points inside the ABCD quadrangle in Fig. 2, the defect formation energy is located between the maximum and minimum values for each defect species at A, B, C, and D points. The electron Fermi energy dependent defect formation energies at points A, B, C and D are shown in Fig. 3.

The nominally charged states, 2^-, 4^- and 2^-, are preferred for V_{Sr}, V_{Ti} and Sr_{Ti}, respectively. Conversely, the charge states of the other defects significantly depend on the Fermi energy. The thermodynamic transition levels for V_O, O_i, Sr_i, Ti_i and Ti_{Sr} are shown in Fig. 4. (Here, all thermodynamic transition energies are measured from the VBM). The V_O shows two transitions, which are ($2^+/1^+$) at 2.68 eV and ($1^+/0$) at 2.83 eV. Both O_i and Sr_i exhibit a "negative-*U*" behavior, indicating that its acceptor level is below its donor level and the singly charged defect is unstable at all Fermi levels. The thermodynamic transition energy for O_i from 0 to 2^- is at 1.11 eV, and that of Sr_i from 2^+ to 0 is at 2.60 eV. In the case of Ti_i, four transitions are observed. They are ($4^+/3^+$) at 0.39 eV, ($3^+/2^+$) at 2.67 eV, ($2^+/1^+$) at 2.74 eV and ($1^+/0$) at 3.00 eV. For Ti_{Sr}, the ($2^+/1^+$) and ($1^+/0$) transitions occur at 0.17 eV and 0.29 eV, respectively. Furthermore, the

formation energy of each point defect also depends on the chemical potential, as shown in Fig. 3.

3.2 Formation energies of native defect complexes

Although isolated point defects may exist in charged states, the overall crystal must be neutral. The charge compensation between acceptors and donors is an important mechanism for maintaining the overall crystal neutrality and thus requires the consideration of a series of different defect complexes. According to classical models, native defect complexes are described by Frenkel, Schottky and cation antisite defect mechanisms. All native defect complex formation energies are computed using isolated neutral (denoted as N-defect complexes) and/or nominally charged (denoted as C-defect complexes) point defect calculations. In other words, defect complex formation energy is defined as the sum of the formation energies of all of the corresponding isolated defects. Such study does provide the simplification of not having to consider the effect of the Fermi energy.

The calculated formation energies of the native defect complexes are listed in Table II. From Table II, it can be seen that the relative stability of each defect complex depends on the charge states of the isolated defects within the complex. For *N*-defect complexes, the magnitudes of the formation energies have the following sequence: O Frenkel < Schottky < Cation Antisite < Sr Frenkel < Ti Frenkel. In the case of *C*-defect complexes, the sequence of formation energies is: Schottky < O Frenkel < Sr Frenkel < Ti Frenkel < Cation Antisite. Furthermore, the formation energies of the native defect complexes consisting of nominally charged isolated defects are lower than those consisting of neutral or partially charged (not included in Table II) isolated defects. Therefore, the defect complexes comprise of nominally charged isolated defects will dominate, with the Schottky defect complex consisting of $V_{Sr}^{2-} + V_{Ti}^{4-} + 3V_{O}^{2+}$ being the most

stable defect structure.

We now compare our results to a previous semi-empirical interatomic potential (SIP) study [16]. In this previous study, all isolated point defects were nominally charged, and thus comparable to our *C*-defect complexes, as shown in Table II. Both the present DFT study and the previous SIP study predict that Schottky and O Frenkel defects have the lowest and the second lowest formation energies, respectively. The formation energies of defect complexes obtained from DFT and SIP methods show a similar trend, although the SIP results for the Sr and Ti Frenkel pairs agree only qualitatively with our DFT results. Compared to our DFT results, the previous SIP results underestimated the formation energy of the Sr Frenkel defect by 1.21 eV/defect and overestimated that of the Ti Frenkel pair by 1.44 eV/defect. For the cation antisite defect, a comparison is not possible due to the absence of similar results in the SIP study.

From the calculated formation energies (Table II), the concentration of each native defect complex can be determined according to the Arrhenius formula as follows:

$$C_d = N_{site} N_{config} \exp(-E_f / k_B T) \quad , \tag{6}$$

where N_{site} and N_{config} are the numbers of sites per unit volume and of equivalent configurations for the defect, k_B is the Boltzmann constant and T is the temperature. The calculated temperature dependent concentrations of various *C*-defect complexes of $SrTiO_3$ are shown in Fig. 5. Based on these results, it is concluded that only these native defect complexes, i.e. Schottky and O Frenkel, which have relatively low formation energies would be present in a material and thus have practical implications. For instance, when the formation energy of a particular native defect complex type (Sr Frenkel, Ti Frenkel and Antisite) is larger than 5 eV/defect, the concentration will be less than 1 cm^{-3} even at 1200 K. These native defect complexes would, therefore, be unlikely under real experimental conditions.

3.3 Defect complexes in nonstoichiometric $SrTiO_3$

The defect complexes in nonstoichiometric $SrTiO_3$ are studied in order to guide the experimental growth of $SrTiO_3$. Corresponding to the chemical compositions of SrO and TiO_2, two possible nonstoichiometric mechanisms are considered, i.e. excess SrO and excess TiO_2. The chemical potentials of elements in the cases of excess SrO and excess TiO_2 are indicated by the lines CD and AB in Fig. 2, respectively. In this section, only nominally-charged, intrinsic point defects are involved in the possible defect formation reactions. Table III lists the defect formation reactions and their respective reaction enthalpies (ΔH); defined as the energy difference of the compounds/defects between the right and left sides of each reaction coordinate.

By analyzing all reactions in Table III, several conclusions can be reached. In the case of excess SrO, reaction 2 (R2), has the lowest ΔH and therefore its products, V_O^{2+} and Sr_{Ti}^{2-}, will be the dominant defect species. The reaction enthalpy of R3, which involves the Sr_{Ti}^{2-} and Sr_i^{2+}, is also relatively low and its products would be the second most prevalent defects. Other defect formation reactions, i.e. R1, R4 and R5, are less likely due to their very high reaction enthalpies. Under TiO_2 rich conditions, R8 and R9, which involve V_{Sr}^{2-} together with Ti_{Sr}^{2+} or V_O^{2+}, have the lowest reaction enthalpies. As such, it can be concluded that excess TiO_2 will lead to V_{Sr}^{2-} together with Ti_{Sr}^{2+} and V_O^{2+} as the most probable defects. The reaction enthalpies of R7 and R10 are also relatively low, indicating the possibility of O_i^{2-} and Ti_i^{4+} defects. The reaction R6 is unlikely, since its reaction enthalpy is high (up to 15.16 eV). The temperature dependent concentrations of the final defects in each reaction are provided in Fig. 6 (a) and (b) for a quantitative description.

In nonstoichiometric $SrTiO_3$ with excess SrO or TiO_2, the possible defect reactions play a key role in determining the type and concentrations of point defects created during the synthesis process. This is especially important for oxygen vacancies, as they are known to be intimately related to desirable functionalities in $SrTiO_3$. As indicated by R2 and R9, both excess SrO and TiO_2 growth conditions induce additional oxygen vacancies. Our calculations suggest that nonstoichiometric chemical compositions, with either excess SrO or TiO_2, could be used to fabricate $SrTiO_3$ in order to maximize oxygen vacancies. Another point that should be considered is the fact that cation antisite defects are energetically unfavorable in stoichiometric $SrTiO_3$ but form readily in nonstoichiometric $SrTiO_3$, i.e. Sr_{Ti}^{2-} and Ti_{Sr}^{2+} in SrO-rich (R2) and TiO_2-rich (R8) environments, respectively. Accordingly, the type and concentration of cation antisite defect could also be controlled by adjusting the amount of excess SrO or TiO_2. Meanwhile, a small concentration of O_i^{2-} and Ti_i^{4+} defects together with a high concentration of V_{Sr}^{2-} will appear under TiO_2 excess conditions (R7, R10 and R9, respectively); while lower concentrations of Sr_i^{2+} will form in excess SrO (R3). Lastly, the reaction enthalpies for R8 and R9 are lower than that of R2, indicating that a TiO_2-rich environment is energetically more favorable than excess SrO in $SrTiO_3$ crystals. In experiments, $SrTiO_3$ samples may have different intrinsic defect structures because of various experimental conditions and therefore show different properties. The intrinsic defect structures discussed here are expected to provide insights for understanding the discrepancy in defect types/concentrations and hence the related performance of $SrTiO_3$ synthesized under various conditions. Based on the present theoretical results, the control of defect structures in $SrTiO_3$ could be achieved by tuning the processing conditions; thereby providing a route by which the functionality and performance of $SrTiO_3$ can

be optimized.

4 Conclusions

The energetics of point defects in stoichiometric and nonstoichiometric $SrTiO_3$ has been comprehensively investigated using DFT calculations. The formation energies of isolated intrinsic point defects depend on both the electron Fermi energy and the element chemical potentials. It is found that the charge states of V_O (2+/1+/0), O_i (0/2-), Sr_i (2+/0), Ti_i (4+/3+/2+/1+/0) and Ti_{Sr} (2+/1+) change as a function of electron Fermi energy, while V_{Sr}, V_{Ti} and Sr_{Ti} prefer their nominal charge states (2-, 4- and 2-, respectively) across the entire band gap.

The formation energies of native defect complexes are found to be related to the charge states of their corresponding intrinsic point defects. The defect complexes comprised of nominally charged defects have lower formation energies than those consisting neutral and partially charged defects. Among the nominally charged-defect complexes, the Schottky defect complex ($V_{Sr}^{2-} + V_{Ti}^{4-} + 3V_O^{2+}$), which has the lowest formation energy, is found to be the most stable defect structure, while the O Frenkel defect complex may also occur as a result of its relatively low formation energy.

Nonstoichiometry, such as excess SrO or TiO_2 in $SrTiO_3$, results in different point defect complexes. For excess SrO, the formation of V_O^{2+} and Sr_{Ti}^{2-} is energetically favorable, while the V_{Sr}^{2-} together with Ti_{Sr}^{2+} and V_O^{2+} are the predominant defects found in excess TiO_2 environments. An excess of both SrO and TiO_2 leads to an increase in the concentration of oxygen vacancies. Similarly, Sr_{Ti}^{2-} and Ti_{Sr}^{2+} antisite defects will appear under SrO-rich and TiO_2-rich conditions, respectively. It is expected that these results will provide guidelines for controlling processing

conditions in order to optimize functionalities bases on specific defects.

Acknowledgements

This work was supported by the U.S. Department of Energy, Basic Energy Sciences, Materials Science and Engineering Division. This research used resources of the National Energy Research Scientific Computing Center, which is supported by the Office of Science, U.S. Department of Energy under Contract No.DEAC02-05CH11231.

References:

[1] G. D. Wilk, R. M. Wallace and J. M. Anthony, *J. Appl. Phys.*, 2001, **89**, 5243.

[2] S. L. Swartz, *IEEE Trans. Electr. Insul.*, 1990, **25**, 935.

[3] C. Aruta, *Phys. Status Solidi A*, 2001, **183**, 353.

[4] A. Kosola, M. Putkonen, L. S. Johansson and L. Niinistö, *Appl. Surf. Sci.* 2003, **211**, 102.

[5] W. J. Weber, R. C. Ewing, C. R. A. Catlow, T. Diaz de la Rubia, L. W. Hobbs, C. Kinoshita, Hj. Matzke, A. T. Motta, M. Nastasi, E. K. H. Salje, E. R. Vance and S. J. Zinkle, *J. Mater. Res.*, 1998, **13**, 1434.

[6] D. Kan, T. Terashima, R. Kanda, A. Masuno, K. Tanaka, S. Chu, H. Kan, A. Ishizumi, Y. Kanemitsu, Y. Shimakawa and M. Takan , *Nat. Mater.*, 2005, **4**, 816 .

[7] M. Choi, F. Oba, Y. Kumagai and I. Tanaka, *Adv. Mater.*, 2013, **25**, 86.

[8] O. N. Tufte and P. W. Chapman, *Phys. Rev.*, 1967, **155**, 796.

[9] A. Ohtomo and H. Y. Hwang, *J. Appl. Phys.*, 2007, **102**, 083704.

[10] M .Cho, F. Oba and I. Tanaka, *Phys. Rev. Lett.*, 2009, **103**, 185502.

[11] N. H. Chan, R. K. Sharma and D. M. Smyth, *J. Electochem. Soc.*, 1981, **128**, 1762.

[12] N. A. Benedek, A. L. S. Chua, C. Elsasser, A. P. Sutton and M. W. Finnis, *Phys. Rev. B*, 2008, **78**, 064110.

[13] K. J. Dudeck, N. A. Benedek, M. W. Finnis and D. J. H. Cockayne, *Phys. Rev. B*, 2010, **81**, 134109.

[14] M. Kim, G. Duscher, N. D. Browing, K. Sohlberg, S. T. Pantelides and S. J. Pennycook, *Phys. Rev. Lett.*, 2001, **86**, 4056.

[15] B. Liu, V. R. Cooper, Y. Zhang and W. J. Weber, To be submitted.

[16] M. J. Akhtar, Z. Akhtar, R. A. Jackson and C. R. A. Catlow, *J. Am. Ceram. Soc.*, 1995, **78**, 421.

[17] J. Crawford and P. Jacobs, *J. Solid State Chem.*, 1999, **144**, 423.

[18] T. Tanaka, K. Matsunaga, Y. Ikuhara and T. Yamamoto, *Phys Rev B*, 2003, **68**, 205213.

[19] G. Kresse and D. Joubert, *Phys. Rev. B*, 1999, **59**, 1758.

[20] J. P. Perdew, K. Burke and M. Ernzerhof, *Phys. Rev. Lett.*, 1996, **77**, 3865.

[21] A. I. Liechtenstein, V. I. Anisimov and J. Zaanen, *Phys.Rev. B*, 1995, **52**, R5467.

[22] S. Okamoto, A. J. Millis and N. A. Spaldin, *Phys. Rev. Lett.*, 2006, **97**, 056802.

[23] H. J. Monkhorst and J. D. Pack, *Phys. Rev. B*, 1976, **13**, 5188.

[24] W. Luo, W. Duan, S. G. Louie and M. L. Cohen, *Phys. Rev. B*, 2004, **70**, 214109.

[25] K. van Benthem, C. Elsässer and R. H. French, *J. Appl. Phys.*, 2001, **90**, 6156.

[26] S. B. Zhang, S. H. Wei and A. Zunger, *Phys. Rev. B*, 2005, **16**, 9642.

[27] F. Oba, M. Choi, A. Togo and I. Tanaka, *Sci. Technol. Adv. Mater.*, 2011, **12**, 034302.

[28] A. F. Kohan, G. Ceder, D. Morgan and Chris G. Van de Walle, *Phys. Rev. B*, 2000, **61**, 15019.

[29] K. Reuter and M. Scheffler, *Phys. Rev. B*, 2001, **65**, 035406.

[30] B. Liu, J. M. Wang, F. Z. Li, J. Y. Wang and Y. C. Zhou, *J. Am. Ceram. Soc.*, 2012, **95**, 1093.

[31] B. Liu, J. M. Wang, F. Z. Li, L. C. Sun, J. Y. Wang and Y. C. Zhou, *J. Am. Ceram. Soc.*, 2013, **96**, 3304.

[32] H. X. Xu, D. Lee, J. He, S. B. Sinnott, V. Gopalan, V. Dierolf, and S. R. Phillpot, *Phys. Rev. B*, 2008, **78**, 174103.

[33] Z. Li, B. Liu, J. M. Wang, L. C. Sun, J. Y. Wang and Y. C. Zhou, *J. Am. Ceram. Soc.*, 2012, **95**, 3628.

[34] B Liu, HY Xiao, Y Zhang, DS Aidhy, WJ Weber, *J. Phys.: Condens. Matter*, 2013, **25**, 485003.

Table I Chemical potentials ($-\mu_{Sr}$, $-\mu_{Ti}$, $-\mu_{O}$) of Sr, Ti and O at the corner points, A, B, C and D, in Figure 2.

	$-\mu_{Sr}$	$-\mu_{Ti}$	$-\mu_{O}$
A: Ti- & TiO_2-rich	1.86	0	4.75
B: O- & TiO_2-rich	6.61	9.50	0
C: O- & SrO-rich	5.49	10.62	0
D: Ti- & SrO-rich	0.18	0	5.31

Table II Native defect complex mechanisms and their formation energies (E_f, in eV/defect) where neutral and nominally charged isolated point defects are denoted as *N*- and *C*-defect complexes, respectively. The values in bracket are from Ref. [16].

	N-defect complex	E_f	*C*-defect complex	E_f
Schottky	$0 \leftrightarrow V_{Sr}^{0} + V_{Ti}^{0} + 3V_{O}^{0} + SrTiO_3$	5.73	$0 \leftrightarrow V_{Sr}^{2-} + V_{Ti}^{4-} + 3V_{O}^{2+} + SrTiO_3$	1.64 (1.61)
Sr Frenkel	$Sr_{Sr}^{0} \leftrightarrow V_{Sr}^{0} + Sr_{i}^{0}$	8.31	$Sr_{Sr}^{0} \leftrightarrow V_{Sr}^{2-} + Sr_{i}^{2+}$	5.15 (3.94)
Ti Frenkel	$Ti_{Ti}^{0} \leftrightarrow V_{Ti}^{0} + Ti_{i}^{0}$	11.20	$Ti_{Ti}^{0} \leftrightarrow V_{Ti}^{4-} + Ti_{i}^{4+}$	5.66 (7.10)
O Frenkel	$O_{O}^{0} \leftrightarrow V_{O}^{0} + O_{i}^{0}$	4.43	$O_{O}^{0} \leftrightarrow V_{O}^{2+} + O_{i}^{2-}$	2.55 (2.57)
Antisite	$Sr_{Sr}^{0} + Ti_{Ti}^{0} \leftrightarrow Sr_{Ti}^{0} + Ti_{Sr}^{0}$	6.43	$Sr_{Sr}^{0} + Ti_{Ti}^{0} \leftrightarrow Sr_{Ti}^{2-} + Ti_{Sr}^{2+}$	5.93

Table III Reaction enthalpies (ΔH, in eV) of $SrTiO_3$ nonstoichiometric mechanisms under SrO- (line CD in Fig. 2) and TiO_2- (line AB in Fig. 2) rich conditions; R: reaction.

Nonstoichiometric mechanisms	ΔH (eV)
SrO-rich:	
R1. $SrO \leftrightarrow Sr_i^{2+} + O_i^{2-}$	12.42
R2. $SrO + \frac{1}{2}Ti_{Ti}^{0} + \frac{1}{2}O_O^0 \leftrightarrow \frac{1}{2}SrTiO_3 + \frac{1}{2}V_O^{2+} + \frac{1}{2}Sr_{Ti}^{2-}$	2.89
R3. $SrO + \frac{1}{3}Ti_{Ti}^{0} \leftrightarrow \frac{1}{3}SrTiO_3 + \frac{1}{3}Sr_{Ti}^{2-} + \frac{1}{3}Sr_i^{2+}$	4.37
R4. $SrO + Ti_{Ti}^{0} + 2O_O^0 \leftrightarrow SrTiO_3 + V_{Ti}^{4-} + 2V_O^{2+}$	5.24
R5. $SrO + \frac{1}{3}Ti_{Ti}^{0} \leftrightarrow \frac{1}{3}SrTiO_3 + \frac{1}{3}V_{Ti}^{4-} + \frac{2}{3}Sr_i^{2+}$	6.63
TiO_2-rich:	
R6. $TiO_2 \leftrightarrow Ti_i^{4+} + 2O_i^{2-}$	15.16
R7. $TiO_2 + \frac{1}{2}Sr_{Sr}^{0} \leftrightarrow \frac{1}{2}SrTiO_3 + \frac{1}{2}Ti_{Sr}^{2+} + \frac{1}{2}O_i^{2-}$	4.47
R8. $TiO_2 + \frac{2}{3}Sr_{Sr}^{0} \leftrightarrow \frac{2}{3}SrTiO_3 + \frac{1}{3}Ti_{Sr}^{2+} + \frac{1}{3}V_{Sr}^{2-}$	1.90
R9. $TiO_2 + Sr_{Sr}^{0} + O_O^0 \leftrightarrow SrTiO_3 + V_{Sr}^{2-} + V_O^{2+}$	1.85
R10. $TiO_2 + \frac{2}{3}Sr_{Sr}^{0} \leftrightarrow \frac{2}{3}SrTiO_3 + \frac{1}{3}Ti_i^{4+} + \frac{2}{3}V_{Sr}^{2-}$	2.89

Figure captions

Fig. 1 Interstitial configurations in SrTiO3, view along <010>: (a) an oxygen split-interstitial along <100> (in red), (b) a strontium split-interstitial along <111> (in blue) and (c) a titanium interstitial occupying a bridge position between two Sr sites (in green).

Fig. 2 Chemical potential diagram of Sr-Ti-O, where $SrTiO_3$ is stable in quadrangle ABCD area.

Fig. 3 Electron Fermi level dependent defect formation energies for charged isolated point defects under (a) Ti- & TiO_2- rich, (b) O- & TiO_2- rich, (c) O- & SrO- rich, and (d) Ti- & SrO-rich conditions.

Fig. 4 Thermodynamic transition levels of V_O, O_i, Sr_i, Ti_i and Ti_{Sr}.

Fig. 5 Temperature dependent concentrations of various charged native defect complexes of $SrTiO_3$.

Fig. 6 Temperature dependent concentrations of various defect complexes under (a) SrO-rich and (b) TiO_2-rich conditions.

Graphical Abstract

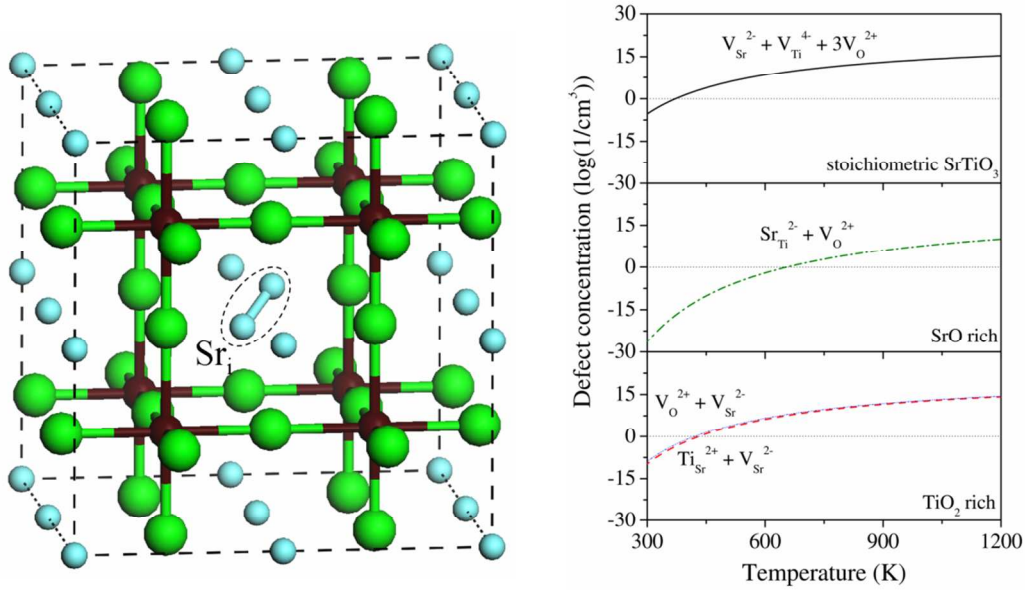

Sr/Ti composition dependent intrinsic defect complexes are predicted, which provide guidelines for optimizing the functionality of $SrTiO_3$ in experiments.